Quaternary Science Reviews 341 (2024) 108840

Contents lists available at ScienceDirect

Quaternary Science Reviews

journal homepage: www.elsevier.com/locate/quascirev

Holocene warmth explains the Little Ice Age advance of Sermeq Kujalleq

Karita Kajanto [a,*], Camilla Andresen [b,a], Helene Seroussi [c], Therese Rieckh [a], Jason P. Briner [d], Basile de Fleurian [a], Andreas Born [a], Kerim Nisancioglu [a]

[a] Department of Earth Science, University of Bergen and Bjerknes Centre for Climate Research, Jahnebakken 5, Bergen, 5007, Norway
[b] Department of Glaciology and Climate, Geological Survey of Denmark and Greenland, Øster Voldgade 10, Copenhagen, 1350, Denmark
[c] Thayer School of Engineering, Dartmouth College, 15 Thayer Drive, Hanover, 03755, NH, USA
[d] Department of Geology, University at Buffalo, 126 Cooke Hall, Buffalo, 14260, NY, USA

ARTICLE INFO

Handling Editor: Qiuzhen Yin

Keywords:
Little Ice Age
Glacier advance
Ice sheet rheology
Sermeq Kujalleq
Jakobhsavn Isbræ
Holocene

ABSTRACT

Our understanding of the processes driving the sea-level contribution of fast-flowing marine-terminating glaciers of the Greenland ice sheet is largely based on observations from the 20th century, with a large bias towards retreating glaciers. The pre-industrial extent of the ice edge is preconditioned by the long and warm Holocene period (from 9700 BCE), followed by a cooling culminating in the Little Ice Age (1250–1900 CE). To improve our understanding of ice dynamics, the evolution of rapidly flowing outlet glaciers should be reviewed in the context of centennial to millennial scale climate variability. Using proxy records and a numerical ice sheet model, we reconstruct the advance of Sermeq Kujalleq (Jakobshavn Isbrae) during the Little Ice Age. We find that the recorded extent of the advance requires an upstream source of soft and deformable ice, combined with reduced calving at the front. We highlight that the Little Ice Age marks the maximum extent of the glacier, following a longer, centennial, period of advance. The subsequent retreat of the glacier front from the Little Ice Age overlaps with the current period of Anthropogenic climate warming, making it difficult to disentangle the Anthropogenic contribution to the 20th century retreat.

1. Introduction

Dynamic changes in marine-terminating glaciers currently contribute to approximately half of the present-day mass loss from the Greenland ice sheet (Mouginot et al., 2019), and are thus important contributors to global sea-level rise. The processes governing the evolution of marine-terminating glaciers remain uncertain; however, significant progress has been made by combining glacier modelling, fjord circulation modelling, field data and satellite observations (Murray et al., 2015; Benn et al., 2017; Catania et al., 2020; Wood et al., 2021). Our improved understanding of these physical processes has been applied in dynamic glacier models (Nowicki et al., 2020), which have been further tuned with observational data since the pre-industrial (1850 CE). However, this is a period dominated by glacier retreat, and as a consequence, there is a risk that the simulated response of the glaciers to climate change is biased by processes operating at decadal time scales and towards periods of glacier retreat.

Following the peak Holocene warmth, climate over Greenland has cooled for the past 5000 years — the Neoglacial cooling — causing widespread, but asynchronous and region-dependent advance of outlet glaciers from their mid-Holocene minimum extent (Briner et al., 2016; Kjær et al., 2022). The general cooling trend of the Neoglacial was broken by an intense warming period; the Roman Warm Period (0–500 CE) (Andresen et al., 2011; Kjær et al., 2022), before the final, short and cold advance period between 1250–1900 CE, commonly known as the Little Ice Age (Kjær et al., 2022) (Fig. 1a). Thus, the pre-industrial extent of the Greenland ice sheet, often used as the starting point for glacier modelling, is a response to a climate cooling event, and does not necessarily represent a stable configuration.

Arguably the best constrained Little Ice Age history of a Greenlandic outlet glacier is that of Sermeq Kujalleq (also known as Jakobshavn Isbrae, Fig. 1b). The retreat of Sermeq Kujalleq from its Little Ice Age maximum extent in 1851 CE to the present-day configuration has been well documented (Bauer, 1968; Weidick et al., 2004; Weidick and Bennike, 2007; Csatho et al., 2008). The Holocene minimum extent of the glacier has been estimated to be 5–10 km inland from the present-day ice front (Weidick et al., 1990; Kajanto et al., 2020), indicating a 40 km advance from the Holocene minimum extent to the Little Ice Age maximum extent. The observed evolution of Sermeq Kujalleq in the recent decades is suggested to have been be triggered at the ice-ocean interface (Bondzio et al., 2018; Khazendar et al., 2019; Joughin et al., 2020), and linked to changes in the temperature of the subsurface Atlantic water in Disko Bay (Gladish et al., 2015; Joughin et al., 2020).

* Corresponding author.
E-mail address: karita.kajanto@uib.no (K. Kajanto).

https://doi.org/10.1016/j.quascirev.2024.108840
Received 12 March 2024; Received in revised form 4 July 2024; Accepted 13 July 2024
Available online 9 August 2024

Table 1
Ice rheology and results from areal fit of the ice extent of the models to the reconstructed Little Ice Age extent, with duration of the advance to the best fit of the total area, and coverage of the model compared to reconstructed maximum coverage in each of the sectors at the time of best fit (See Fig. 1).

Model parameters		Best fit to the reconstruction			
Ice rheology	Margins in the fjord	Time (yr)	Fjord (%)	North (%)	South (%)
Cold	No	731	57	164	159
Warm	No	518	82	112	140
Cold	Yes	372	88	112	119
Warm	Yes	407	92	103	119

Reconstructions of the Atlantic water temperature variability based on foraminiferal assemblage changes in sediment cores (Andresen et al., 2010; Moros et al., 2016; Wangner et al., 2018) indicate that the subsurface water in Disko Bay was warm during the Roman Warm Period, comparable to the present-day and the mid-Holocene (Fig. 1a, Fig. S1). The ice rafted debris record in front of the fjord suggests that Sermeq Kujalleq was calving periodically from the Roman Warm Period until 1100 CE, close to the start of the Little Ice Age (Wangner et al., 2018) (Fig. 1a). Both the reconstructed ocean conditions and the record of ice rafted debris support the notion of a retreated extent of Sermeq Kujalleq during the Roman Warm Period, which implies that the advance to the Little Ice Age extent was relatively short in duration. This raises the question: how could the glacier front have advanced so much so fast?

We model the Little Ice Age advance of Sermeq Kujalleq with the Ice-sheet and Sea-level System Model (ISSM) (Larour et al., 2012) under cool climate conditions, representing mean conditions since the Roman Warm Period. We assume as a conservative estimate that the ice front retreated to its Holocene minimum extent during the Roman Warm Period due to warm ocean conditions in Disko Bay. This is a stable configuration of the ice front in the model that can sustain a high calving flux, as indicated by the ice rafted debris record (Fig. 1a). We examine the impact of changes in glacier calving and in the ice flow properties, **rheology**, on the advance, and determine the best ice rheology by evaluating the fit of the modelled advanced ice extent to the reconstructed Little Ice Age extent. We show that the advance was triggered from the ice-ocean interface by a decrease in calving, leading to the formation of a floating ice shelf in the fjord. Furthermore, our results show that soft and deformable ice, combined with significant shear margin softening, is essential in order to create the extent and shape of the Little Ice Age ice front of Sermeq Kujalleq.

2. Model setup and methods

2.1. Ice-flow model

We use the Ice-sheet and Sea-level System Model (ISSM) (Larour et al., 2012), in a two-dimensional setup described in Kajanto et al. (2020), with the Shelfy Stream Approximation (Morland, 1987; MacAyeal, 1989). Migration of the calving front is tracked with the level-set method (Bondzio et al., 2016), and the grounding line evolves according to the sub-element hydrostatic scheme (Seroussi et al., 2014). The mesh is a non-uniform triangular mesh with a resolution varying from 10 km inland down to 200 m in the fjord and the deep trough. Sliding follows the sliding law from Budd et al. (1979) with two values for basal friction: a low value of 20 $(s/m)^{1/2}$ for deep areas in the fjord and trough, and a higher value of 50 $(s/m)^{1/2}$ for the rest of the domain. The values correspond to the average values for the respective regions obtained from inverting the present-day surface velocity (Larour et al., 2012; Seroussi et al., 2013). Thus, we assume that the basal properties are not significantly different from present-day values during the studied time period, and that topography dominates the basal properties as softer sediments are accumulated to the deep troughs. This is a simplification that is made primarily due to the lack of data, and we consider it a reasonable assumption during most of the studied time period. During the coldest period of the Little Ice Age, however, there was likely less subglacial discharge, and thus potentially less deformation and sliding at the bed, leading to slower advance. This is in line with other assumptions in our model, as we provide a lower limit to the advance duration. We also exclude the impact of sediment accumulation at the base due to uncertainty, although we presume that the sediment flux in a colder climate than the present-day sediment flux of 0,084 Gt yr^{-1} of the Sermeq Kujalleq catchment (Andresen et al., 2024). This indicates relatively low deposition volumes compared to the depth of the grounding line and the error within the bedrock topography (Morlighem et al., 2017).

The model is initialized from the inner limit of the Holocene minimum extent of Sermeq Kujalleq (yellow line in Fig. 2), determined in Kajanto et al. (2020), where the front and the grounding line of the main trunk are stable at a location approximately 5 km inland from the estimated 2012 extent (Time slice 7500 BP of experiment SE_SM in Kajanto et al. (2020)). Bedrock topography is updated to BedMachine v5 (Morlighem et al., 2017) and relative sea level considerations are excluded, since they are expected to be less than 10 m during the time of interest of this study (Long et al., 2006). We keep the same approach to construct surface mass balance as in Kajanto et al. (2020), by imposing variations in the equilibrium line altitude (ELA) (Helsen et al., 2012). The vertical SMB gradients are calculated from a reference SMB: a pre-industrial global NorESM boundary climate with regionality adapted from MAR, as in Plach et al. (2018). The spinup is ran with a present-day equivalent ELA of 1200 m. The cold atmospheric forcing of the experiments uses ELA of 1000 m (also used in Kajanto et al., 2020 for Little Ice Age climate). Initial testing with a colder ELA of 800 m resulted in significantly worse areal fit due to excessive advance of the terrestrial margins.

During the warm climate conditions of the spinup, we assume a present-day like, piecewise linear vertical melt rate profile along the glacier front, where the upper water layer extends down to 100 m depth, while the deepwater layer is below 400 m depth (Kajanto et al., 2023). The upperwater melt rate is kept constant at a low value of 10 m/yr, while the deepwater melt rate is 50 m/yr. During the cold climate conditions of the experiments the submarine melt rate is constant at 10 m/yr along the front, with negligible impact to the results.

We spin the ISSM model up by running the initial configuration for 1000 years with constant warm climate conditions and net mass loss, using either the cold or warm ice rheology (Fig. S3). We then run the model forward, changing linearly from the warm climate conditions to the cold conditions within the first 100 years of the experiment, and run the model until the ice extent reaches the best fit with the reconstructed Little Ice Age margin, or up to 1000 years (blue shading in Fig. 3). We do this for both cold and warm ice, testing the fit with a range of calving thresholds and shear margin softenings (Table S1), and present results for the best experiment (Figs. 2, 3) and the comparison with other rheology alternatives (Table 1). Best fit is determined by when the total surface area covered by the modelled ice mask in the three test sectors equals to the surface area covered by the reconstruction within the sectors (mesh elements within the reconstruction). We then examine the coverage of modelled ice within each of the three test sectors to the reconstructed coverage, in order to separate the advance of the fjord sector and the terrestrial margins (blue outlines in Fig. 1b).

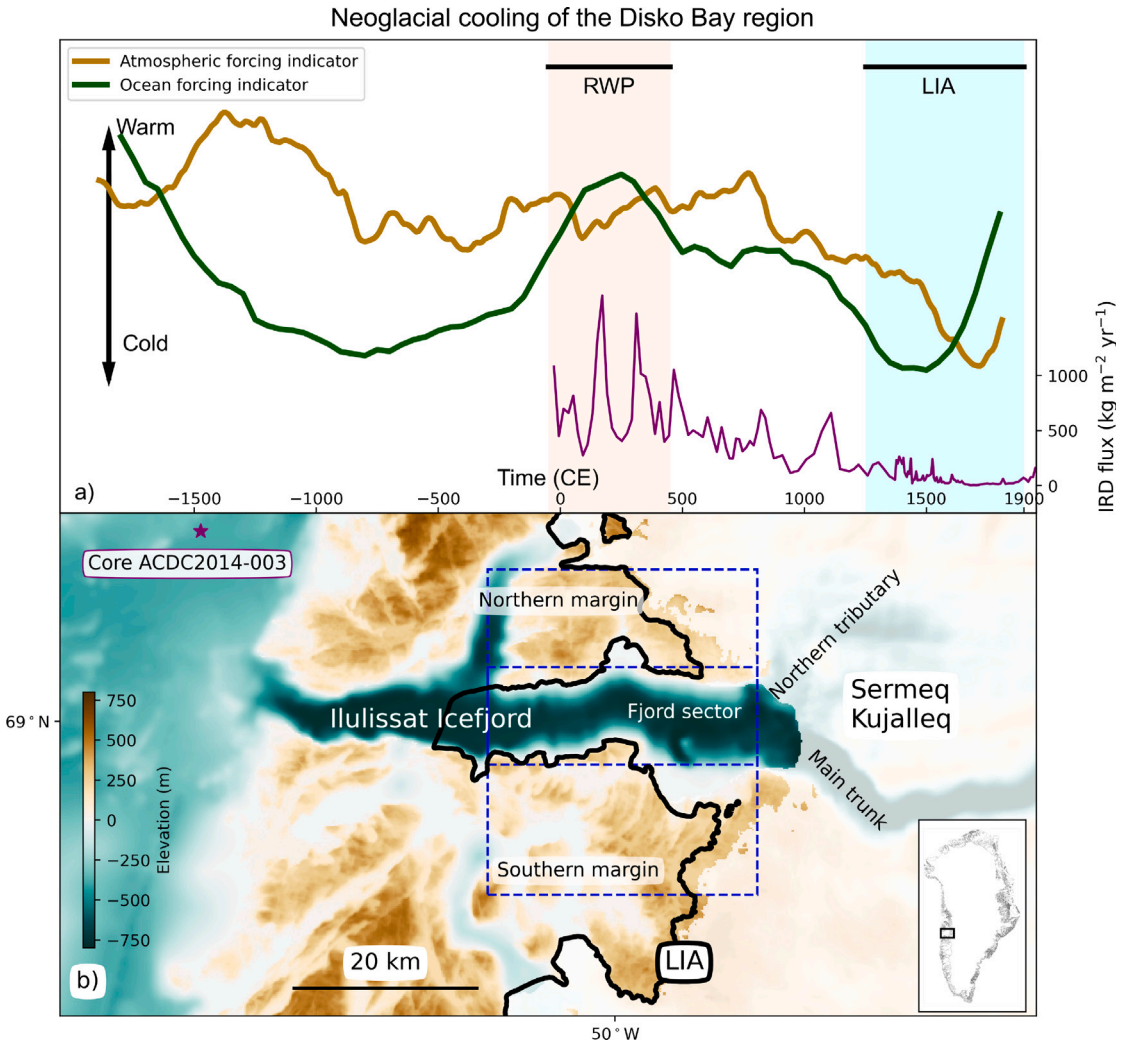

Fig. 1. (a) Proxy compilations indicating the relative evolution of atmospheric temperature over Greenland (brown line, Vinther et al., 2009; Kobashi et al., 2011, see Fig. S1 for details) and subsurface water temperature in the Disko Bay area (green line, Moros et al., 2016; Wangner et al., 2018 see Fig. S1 for details) during the last 4000 years of the Neoglacial. Black horizontal lines and shading indicate the timing of the Roman Warm Period (RWP, light orange) and the Little Ice Age (LIA, light blue) (Kjær et al., 2022). The ice rafted debris (IRD) flux from core ACDC2014-003 (purple line, Wangner et al., 2018), showing the shift from the RWP high-IRD-flux climate to the LIA climate with low IRD. (b) Bathymetry and topography of the Ilulissat Icefjord and Sermeq Kujalleq frontal region (green-to-brown, only indicative inside the present-day ice mask, BedMachine v5 Morlighem et al., 2017), naming of the different sectors and the present-day ice mask (white shading, BedMachine v5 (Morlighem et al., 2017)). We outline in black the maximum extent of the Little Ice Age advance drawing from our own fieldwork and from previously published maps (Weidick and Bennike, 2007; Csatho et al., 2008; Briner et al., 2010). The blue boxes indicate the areas used for areal fitting of the modelled ice front in Table 1. Purple star indicates the core location for IRD data.

2.2. Calving

We use the von Mises calving criterion (Morlighem et al., 2016), where the calving front is advected at a velocity:

$$v_{\text{front}} = \mathbf{v} - \left(c + \dot{M}\right)\mathbf{n}, \tag{1}$$

where $\mathbf{v}$ is the horizontal velocity of the ice, c the calving rate and $\dot{M}$ the rate of undercutting at the calving front, and $\mathbf{n}$ is a unit normal vector that points outward from the ice domain. The calving rate is further defined as:

$$c = \frac{\sigma_{\text{VM}}}{\sigma_{\text{max}}}\|\mathbf{v}\|, \tag{2}$$

where c is the calving rate, σ_{VM} the von Mises tensile stress of the ice, σ_{max} is the maximum allowed "strain rate" in the ice — the calving threshold — and $\|\mathbf{v}\|$ the magnitude of the horizontal ice velocity. This parameterization is controlled by the calving threshold σ_{max}, which is specific for each glacier and has been found to be within the range of 300–1200 kPa for present-day glaciers in West Greenland (Bondzio et al., 2018; Choi et al., 2018; Morlighem et al., 2019). σ_{max} is set separately for grounded and floating ice, but since advance in our model is insensitive to the value for grounded ice, we keep it at a constant value of 1000 kPa, calibrated in Kajanto et al. (2020), and only change the σ_{max} value for floating ice in the experiments. In addition, we impose a constant minimum thickness condition of 80 m, and an undercutting rate of 10 m/yr, both of which are kept constant throughout the runs and have little impact on the results.

The calving threshold for floating ice in Sermeq Kujalleq has been calibrated to have a present-day summer-to-winter range of 50–400 kPa (Bondzio et al., 2018), and an annual mean value of 300 kPa for the Mid-Holocene (Kajanto et al., 2020). We trigger advance by increasing the threshold sufficiently to permit ice shelf formation, as Kajanto et al. (2020) showed that surface mass balance and melt rate changes are not able to create advance, as long as the front is allowed to calve. We increased σ_{max} at 100 kPa intervals, and found the minimum value to permit advance to range between 800–1000 kPa (Table S1). The best fit is obtained with calving threshold 1100 kPa, which we use in the experiments. The calving threshold is somewhat related to ice rheology, as the best fit between ice rheologies varies between 1000–1200 kPa. Due to the very large reconstructed Little Ice Age extent within the

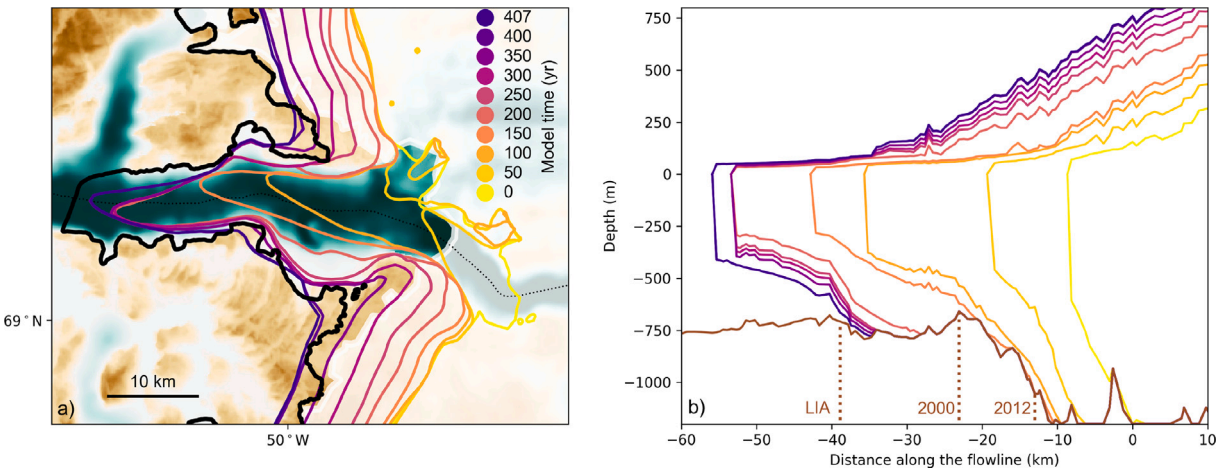

Fig. 2. Modelled evolution of Sermeq Kujalleq during a 400-year advance to the best-fit Little Ice Age extent with warm ice rheology and soft shear margins (See Table 1), plotted at 50-year-intervals (coloured lines, time scale in coloured dots). (a) Ice front position through time and the reconstructed Little Ice Age extent of the glacier (black, Fig. 1). (b) the glacier outline along a flowline along the centerline of the fjord (black dotted line in panel a). The dashed vertical lines in panel (b) indicate the estimated grounding line locations along the flowline at the LIA maximum, at 2000 CE, before the rapid contemporary retreat, and at 2012 CE. The distance along the flowline is computed from the initial grounding line position (presumed Holocene minimum extent). Background is the present-day bathymetry and topography as in Fig. 1 (BedMachine v5 (Morlighem et al., 2017)).

fjord (Fig. 1b), increasing the calving threshold will further improve the fit, since a larger shelf is able to form. However, we require that the southern terrestrial margin must advance before the fjord, as is indicated by the respective advance ages (Briner et al., 2010), which constrains the calving threshold from above (Table S1).

Åkesson et al. (2022) also find that an increase in σ_{max} is necessary to permit shelf formation in Petermann Glacier. However, Sermeq Kujalleq required an order of magnitude larger change in the calving threshold in order to advance, compared to the increase from 300 kPa to 400 kPa for Petermann (Åkesson et al., 2022). The ice shelf in Sermeq Kujalleq needs to be stiff in order to both advance over a relatively wide and deep bathymetry, and to sustain a large degree of shearing from the fjord walls as the velocity within the narrow shelf is high (Fig. 3).

2.3. Ice rheology

We use two different ice temperatures to reconstruct two alternative ice rheologies, called "cold" and "warm" to represent stiff and soft ice. We attribute ice viscosity directly to temperature, since the dependency of the flow parameter A of Glen's flow law to temperature is best established (Cuffey and Paterson, 2010). Other factors can also impact ice viscosity, such as the crystal orientation fabric anisotropy (Gerber et al., 2023), which is not included in the model although likely contributes to the required shear margin softening, as well as impurities within the ice, whose impact on ice deformation remains ambiguous (Stoll et al., 2021), and is thus ignored.

The cold ice rheology is initialized from an ice temperature from Lecavalier et al. (2014) time slice at 9500 yrs BP, interpolated to our model mesh. The warm ice rheology is present-day observed surface temperature lowered by 5 K, as used for present-day Sermeq Kujalleq in Bondzio et al. (2018). The difference of the two temperature fields varies spatially between 6–10 K, the difference being largest close to the front (Fig. S2).

The model setup of Sermeq Kujalleq requires shear margin softening to account for damage in areas with a steep bedrock slope in order to create the rapid flow of the main trunk. The damage factor due to softening has previously been calibrated to 0.5 for present day (Bondzio et al., 2018) and 0.3 for Mid-Holocene (Kajanto et al., 2020). We calibrate the softening value at 0.05 increments based on the areal fit of the advanced ice margin separately for both ice rheologies, resulting to 0.35 for the warm ice rheology and 0.30 for the cold ice rheology (Table S1). For ice outside of the initial ice mask we use a constant viscosity of the ice margin, with or without shear margin softening.

In addition, we impose softening equal to the shear margin softening to the area where the northern tributary merges with the main trunk. Directly before merging, the two branches flow with a significantly different velocity, creating a high strain rate in the zone between the two. Thus, the von Mises tensile stress exceeds the calving threshold (Eq. (2)), and ice between the branches will be calved off and removed from the ice mask. However, we would not expect all ice to be directly removed from between the two shelves, but would expect an area of highly damaged ice to form between the branches. The procedure is similar to Seroussi et al. (2017) model of Thwaites in Antarctica, to handle different flow regimes within a single floating tongue.

2.4. Stratification

The Greenland Ice Sheet stratification is simulated with the coupled ELSA-Yelmo model setup, where ELSA (Englacial Layer Simulation Architecture, (Rieckh et al., 2023; Born and Robinson, 2021)) simulates the englacial stratigraphy and Yelmo is a thermomechanical ice sheet model (Robinson et al., 2020).

The simulation ran from 162000 BP to present day on a regular 8 km Cartesian grid over the entire Greenland ice sheet. Bedrock and ice topography are from Morlighem et al. (2017), the geothermal heat flux field is based on Martos et al. (2018) over land and Shapiro and Ritzwoller (2004) over the ocean. Climate forcing is calculated using a snapshot method using a high-resolution simulation of present-day climate (Fettweis et al., 2017) and global simulations for the last glacial maximum (Abe-Ouchi et al., 2015). Surface mass balance is computed using the positive-degree-day scheme with a snow melt factor of 3 mm K^{-1} d^{-1} water equivalent and ice melt factor of 8 mm K^{-1} d^{-1} water equivalent.

ELSA simulates the englacial stratigraphy of the Greenland ice sheet by modelling individual layers of accumulation explicitly driven by surface mass balance provided by Yelmo. The added layers are isochronal with a resolution of 100 a. Over the course of the simulations and as new layers are added, older layers flow towards the margins and become thinner. Advection occurs exclusively within layers. The parameters of the simulation in Fig. 5 were constrained by direct comparison of a 700-member ensemble with Bedmachine v3 data (Morlighem et al., 2017) and dated radiostratigraphy data (MacGregor et al., 2016) over the entire Greenland domain, at a lower resolution of 16 km.

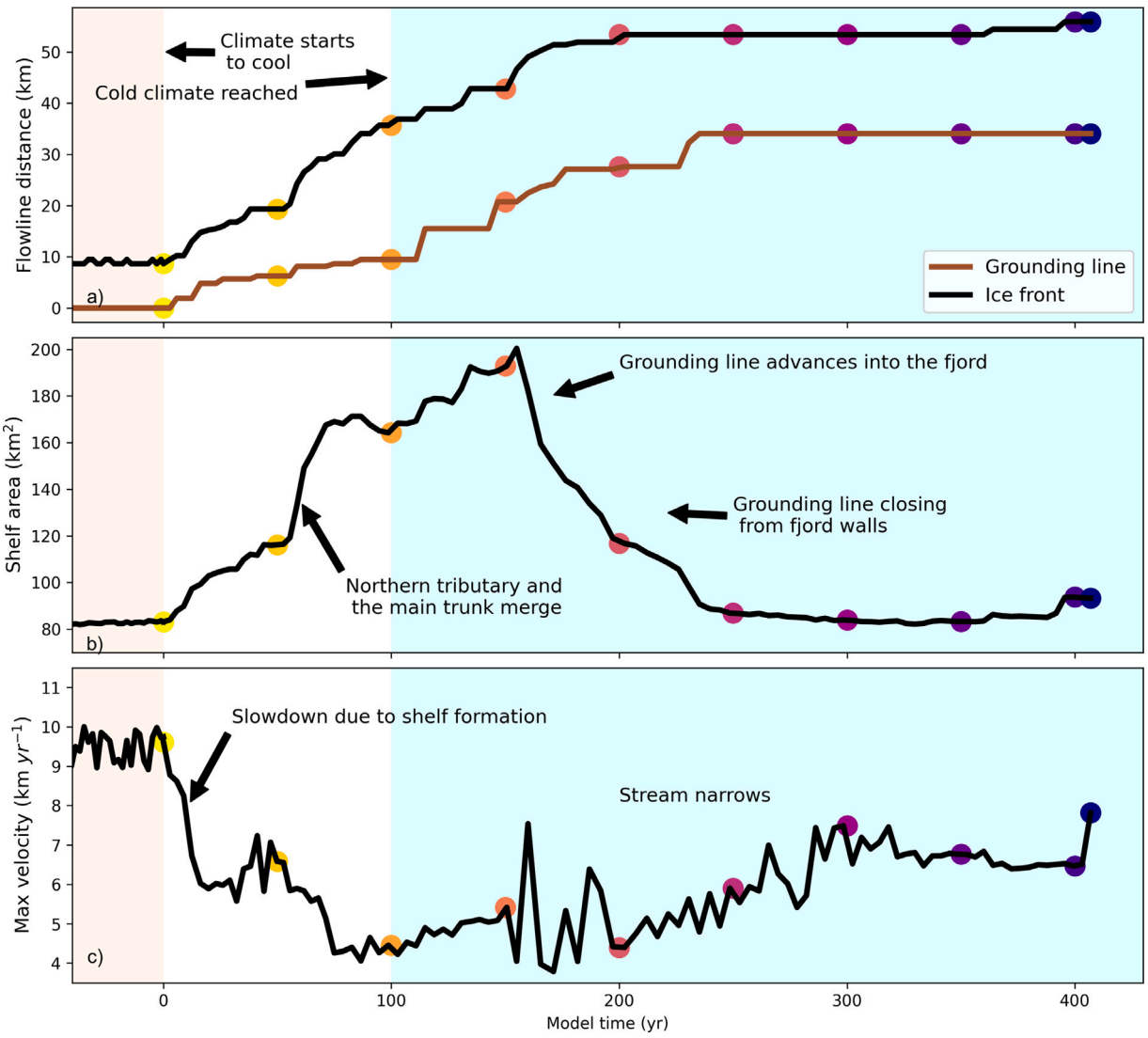

Fig. 3. Evolution of the ice shelf of Sermeq Kujalleq during the advance: (a) Distance of the grounding line (brown) and ice front (black) from the initial grounding line location show the advance and growth of the shelf along the flowline (Fig. 2a). (b) total area of the floating shelf in the catchment demonstrates the growth and narrowing of the shelf. (c) the maximum velocity of the glacier, typically at the calving front, adjusts to changes in the shelf shape. Light orange background colour indicates warm, mass-loss climate of the spinup, light blue background indicates the cold, mass-gain climate of the experiment. Forcing changes linearly within the first 100 years of the experiment, see Methods for details. Coloured circles indicate outline locations plotted in Fig. 2.

3. Results and discussion

3.1. The little ice age advance of Sermeq Kujalleq

We initialize our model experiment from a retreated ice front configuration of Sermeq Kujalleq, approximately 5 km inland from the present-day extent, as suggested in Kajanto et al. (2020) (yellow outline in Fig. 2). Within the first 100 years of the experiment, atmospheric forcing, melt rate and calving change linearly from warm to cold values (see Methods for details). In our model setup, calving is represented by a single parameter — the calving threshold — which controls how easily ice breaks under stress (von Mises calving, see Methods for details). Initially, the calving threshold is at a warm-climate value for Sermeq Kujalleq (Bondzio et al., 2017; Kajanto et al., 2020), creating a high calving flux that maintains a high velocity at the front (Fig. 3c).

As the climate cools, the changing calving condition permits ice shelf formation, which is directly followed by a slowdown of ice flow (Fig. 3b,c). The slowdown causes ice buildup at the grounding line, rapidly leading to thickening and grounding line advance (Fig. 3a). After 50 years, the northern tributary and the main trunk merge, causing a rapid increase in the ice shelf size and further slowdown of ice flow down to 4 km per year due to increased friction with the fjord walls from the larger shelf (Fig. 3b,c). During the first 100 years, the grounding line in the main trunk gradually advances 10 km up to a shallower bed, as a response to the slowdown and thickening of the glacier (Figs. 2b, 3a).

Between 100–150 years the shelf continues to grow in size and flows slowly, while the grounding line advances along the narrow main trunk (Fig. 3a,b), until the grounding line has reached a position close to the observed grounding line of year 2000 (Fig. 2b). From this position, the shelf advances further into the fjord (Fig. 2). Due to the steep and narrow bathymetry, the advancing shelf starts grounding to the sides of the fjord walls, leading to a rapid decrease of the ice shelf area, and grounding line advance along the flowline (Fig. 3). The shelf adjusts to a narrow configuration and ice velocity slowly increases, as the ice shelf continues to slowly thicken and eventually increase in size (Fig. 3).

Our modelled evolution is compatible with the reconstructed history of the terrestrial margins of the glacier (Briner et al., 2010) and provides further insight into the details of the advance, as we can account for the difference in the timing of the advance of the northern

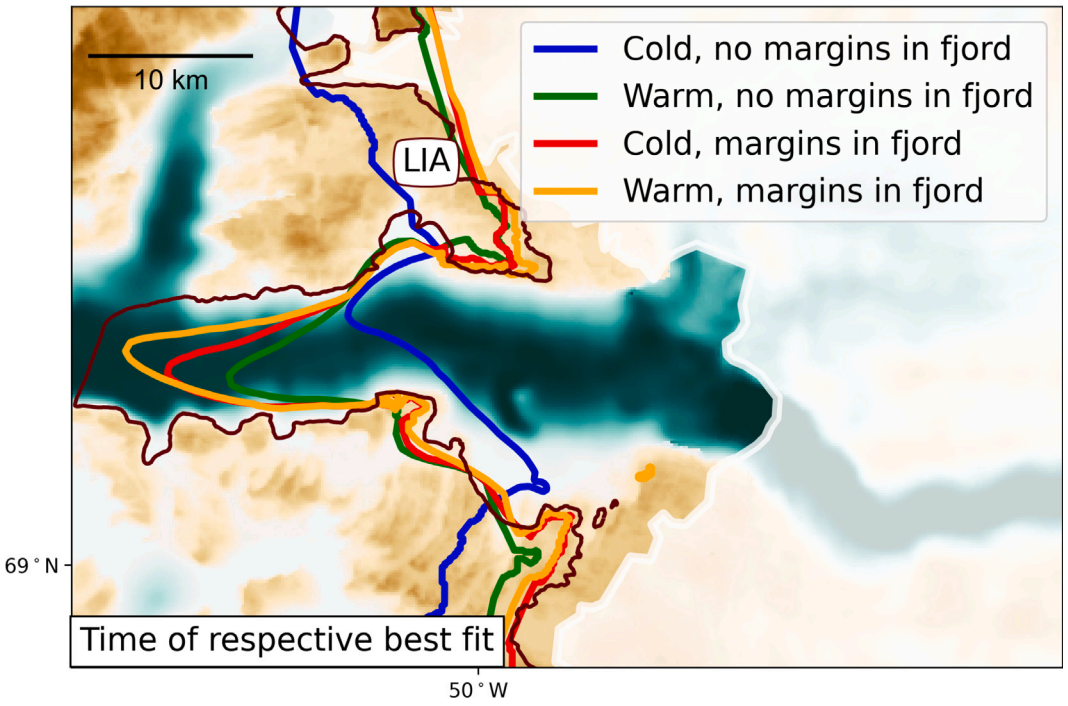

Fig. 4. Glacier outline at the time of respective best areal fit to the reconstructed Little Ice Age extent (dark red outline, see Fig. 1), for the four different ice rheologies presented in Table 1. The times of best fit are listed in Table 1.

and southern terrestrial margins of Sermeq Kujalleq (Fig. 1b). The southern terrestrial margin resides on a topographically high area, where the area inland of the southern margin is also on high terrain Morlighem et al. (2017). For this reason, the southern margin is relatively disconnected from the main trunk of Sermeq Kujalleq, and thus the evidence for a relatively early advance age of 350 BCE of the southern margin Briner et al. (2010) likely reflects a response to the overall cooling trend of the Neoglacial (Fig. 2a).

In contrast to the southern margin, the area directly inland of the northern terrestrial margin is below sea level (Fig. 1b), and we find its advance to the Little Ice Age extent to be directly connected to the advance of the grounding line of Sermeq Kujalleq (Fig. 2). The Little Ice Age advance age of the northern terrestrial margin is 1550–1750 CE (Briner et al., 2010, 2011), indicating that the advance was relatively recent. The last significant peak of the ice rafted debris before the Little Ice Age, indicating significant calving, took place at approximately 1100 CE. If this is taken as the starting point of the advance and the advance age of the northern terrestrial margin as the end point of the advance, the simulated 400-year-advance matches well with the data.

Due to the simplified forcing of our model (See methods), it provides a lower limit to the duration of the advance, demonstrating that the entire evolution from the Holocene minimum to the Little Ice Age maximum extent may have been achieved within 400 years. Thus, our model and the proxy calving data together indicate that the fjord sector of Sermeq Kujalleq remained at a retracted extent — close to the present-day extent — until a rapid advance during the Little Ice Age that was driven by changes at the ice-ocean interface.

3.2. The impact of ice rheology on glacier advance

A significant reduction in calving, in combination with a cool climate, causes mass gain and eventually an advance of Sermeq Kujalleq. However, the fit of the shape of the advanced front to the reconstructed Little Ice Age extent varies significantly depending on the ice rheology (Table 1, Fig. 4). We test two different ice rheologies, representative of warm ice and cold ice (Table 1, see Methods for details). Previous models of Sermeq Kujalleq showed that soft shear margins bordering rapidly flowing areas are essential to match the flow pattern (Bondzio et al., 2018; Kajanto et al., 2020); however, it is uncertain how rapidly shear margins will develop during an advance. Due to this uncertainty, we test two alternatives for the advanced ice rheology: with and without soft shear margins.

In order to test the fit of the modelled ice extent to the reconstruction, we compare the simulated ice-covered area to the field-based reconstruction of the Little Ice Age extent in pre-defined test sectors (areas outlined in blue in Fig. 1b). Cold ice with no shear margins leads to excessive advance of the terrestrial margins and limited advance in the fjord, since the stiff ice does not flow into the fjord (Table 1, Fig. 4). However, warm ice rheology enables a more rapid transport of inland ice towards the front, thus replacing ice lost due to calving at the glacier front and thickening ice at the grounding line. Combining shear margin softening with the cold ice rheology significantly speeds up and improves the fit to the reconstruction, demonstrating the significance of the shear margins (Table 1, Fig. 4). Including soft shear margins in the warm ice rheology gives the best fit to the Little Ice Age reconstruction (Table 1, Fig. 2a). Thus, the extensive advance of the glacier in the fjord compared to the terrestrial margins is achieved by flow of soft ice.

3.3. The evolution of ice rheology in Sermeq Kujalleq

Our model shows that flow of soft ice from inland to the grounding line was a contributing factor to the fast and extensive advance of Sermeq Kujalleq during the Little ice Age climate cooling. The flow properties of the ice are predominantly controlled by the temperature of the ice, making cold ice harder and warm ice softer (Cuffey and Paterson, 2010). The temperature of the ice is determined by the atmospheric forcing at the surface, by the geothermal heating from below and by frictional heating due to internal deformation and basal sliding. During the Holocene, the accumulation and advection of warm Holocene ice into Sermeq Kujalleq has to a large degree replaced the cold glacial ice of the interior, particularly close to the front (Fig. 5). Thus, the long and warm Holocene period preconditions the ice within Sermeq Kujalleq for the rapid advance of the Little Ice Age. This

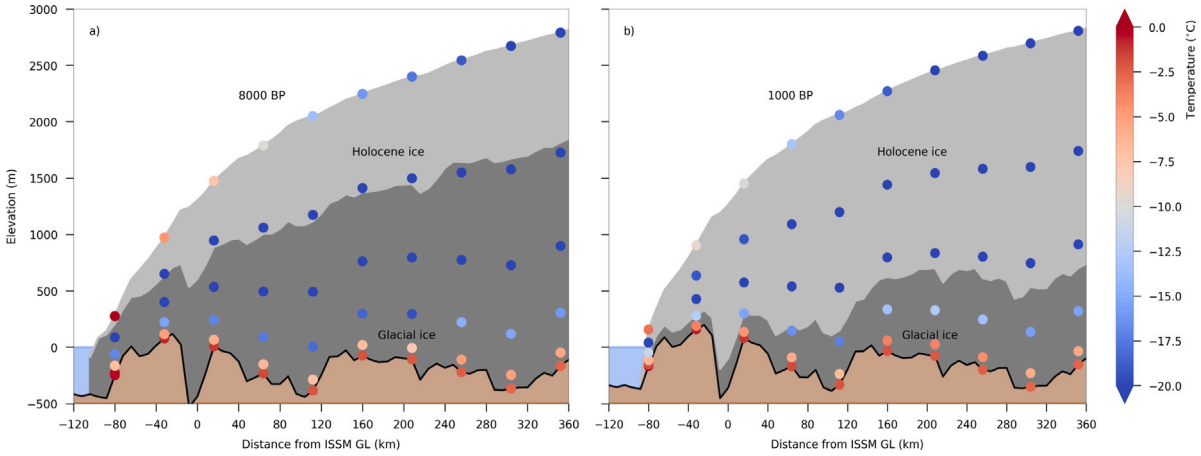

Fig. 5. Accumulation and advection of Holocene ice (light grey shading) and heat (coloured dots) into Sermeq Kujalleq from Mid to Late Holocene, cross-section along 69.1246°N using the ice-sheet model Yelmo (see Methods and Fig. S4 for details). During the Mid-Holocene (left panel), the majority of the ice within the glacier was glacial ice still cold from the preceding ice age. By 1000 yrs BP (right panel), ice accumulated during the Holocene takes up most of the ice volume, and the remaining glacial ice has been heated by up to 6 °C due to geothermal and frictional heating (coloured dots). Note that ISSM and Yelmo are run with different model parameters and boundary conditions (see Methods for details) and are not designed to specifically reproduce each other's results.

demonstrates that a comprehensive understanding of glacier and ice front evolution requires an understanding of their past evolution.

In order to create the advance, we impose a calving condition that causes the ice in the floating shelf to resist calving. We presume that the change in the calving condition encompasses climatic changes influencing the ice-ocean interface, such as decreased runoff from the glacier leading to less hydrofracturing, cooling of the incoming Atlantic Water and potentially changes in the fjord stratification or subglacial discharge. Additionally, the crystal orientation within the ice also has a significant control of the ice rheology (Fan et al., 2020; Gerber et al., 2023). Thus, the anisotropy of the crystal orientation of the ice within Sermeq Kujalleq potentially also contributed to the Little Ice Age advance, with ice being soft for shearing but stiff for along-flow deformation (Gerber et al., 2023).

4. Conclusions

Our study shows that the Little Ice Age extent of Sermeq Kujalleq was facilitated by soft and mobile ice buildup at the grounding line during a relatively short episode of reduced calving. From this perspective, the Little Ice Age extent of the glacier is not representative of a long-term stable extent of the Holocene, but rather the peak extent of a centennial-scale advance episode. Thus, the observed 20th century retreat of Sermeq Kujalleq (Kjeldsen et al., 2015) consists of two components: the recovery from the Little Ice Age climate anomaly and the response to the Anthropogenic warming. It is unclear what are the relative contributions of each component. However, if all retreat since the Little Ice Age maximum is interpreted as Anthropogenic retreat, and glacier models used to assess future sea-level contribution are tuned based on this assumption, there is a risk that the Anthropogenic contribution to the observed 20th century retreat is overestimated. At the same time, the future long-term retreat of Sermeq Kujalleq could be underestimated, as the long-term inherited climate history of the glacier and the upstream ice sheet, as well as processes taking place on centennial to millennial timescales are ignored. From our results follow that the Anthropogenic warming of surface temperature over the Greenland ice sheet will cause further advection of warm ice to Sermeq Kujalleq, promoting faster ice flow and a potential increase in the contribution to global sea-level rise.

Based on our results it is clear that the long-term history of glacier frontal variability and ice rheology must be considered when simulating the future response of glaciers such as Sermeq Kujalleq to Anthropogenic climate change.

CRediT authorship contribution statement

Karita Kajanto: Conceptualization, Designed and conducted the ISSM simulations, Formal analysis, Writing – original draft, Interpretation of the results. **Camilla Andresen:** Conceptualization, Formal analysis, Interpretation of the results. **Helene Seroussi:** Designed and conducted the ISSM simulations, Formal analysis, Interpretation of the results. **Therese Rieckh:** Developed the ELSA model, Ran the simulations, Interpretation of the results. **Jason P. Briner:** Formal analysis, Interpretation of the results. **Basile de Fleurian:** Designed and conducted the ISSM simulations, Interpretation of the results. **Andreas Born:** Developed the ELSA model, Interpretation of the results. **Kerim Nisancioglu:** Conceptualization, Formal analysis, Interpretation of the results.

Declaration of competing interest

The authors declare that they have no known competing financial interests or personal relationships that could have appeared to influence the work reported in this paper.

Data availability

Data will be made available on request.

Acknowledgements

KK and KHN were supported by the European Research Council under the European Community's Seventh Framework Program (FP7/2007-2013) / ERC grant agreement 610055 as part of the ice2ice project and the Research Council of Norway ClimateNarratives grant (NFR 324520). CSA acknowledges funding from the Independent Research Fund Denmark (0217-00244B), the Research Council of Norway (NFR 324520) and the VILLUM Foundation (YIP 10100). HS was funded by grants from NSF Navigating the New Arctic (#2127246) and NOVO Nordisk Foundation (#NNF23OC00807040). TR and AB received funding from the Norwegian Research Council Grant 314614 (Simulating Ice Cores and Englacial Tracers in the Greenland Ice Sheet). The simulations were performed on resources provided by Sigma2—the National Infrastructure for High Performance Computing and Data Storage in Norway.

Appendix A. Supplementary data

Supplementary material related to this article can be found online at https://doi.org/10.1016/j.quascirev.2024.108840.

References

Abe-Ouchi, A., Saito, F., Kageyama, M., Braconnot, P., Harrison, S.P., Lambeck, K., Otto-Bliesner, B.L., Peltier, W.R., Tarasov, L., Peterschmitt, J.Y., Takahashi, K., 2015. Ice-sheet configuration in the CMIP5/PMIP3 Last Glacial Maximum experiments. Geosci. Model Dev. (ISSN: 19919603) 8, 3621–3637. http://dx.doi.org/10.5194/GMD-8-3621-2015.

Åkesson, H., Morlighem, M., Nilsson, J., Stranne, C., Jakobsson, M., 2022. Petermann ice shelf may not recover after a future breakup. Nature Commun. (ISSN: 2041-1723) 13 (1), 1–9. http://dx.doi.org/10.1038/s41467-022-29529-5, URL https://www.nature.com/articles/s41467-022-29529-5.

Andresen, C.S., Karlsson, N.B., Straneo, F., Schmidt, S., Andersen, T.J., Eidam, E.F., Bjørk, A.A., Dartiguemalle, N., Dyke, L.M., Vermassen, F., et al., 2024. Sediment discharge from Greenland's marine-terminating glaciers is linked with surface melt. Nature Commun. 15 (1), 1332.

Andresen, C.S., McCarthy, D.J., Dylmer, C.V., Seidenkrantz, M.S., Kuijpers, A., Lloyd, J.M., 2010. Interaction between subsurface ocean waters and calving of the Jakobshavn Isbræ during the late Holocene. Holocene (ISSN: 09596836) 21, 211–224. http://dx.doi.org/10.1177/0959683610378877, URL https://journals.sagepub.com/doi/10.1177/0959683610378877.

Andresen, C.S., McCarthy, D.J., Dylmer, C.V., Seidenkrantz, M.S., Kuijpers, A., Lloyd, J.M., 2011. Interaction between subsurface ocean waters and calving of the Jakobshavn Isbræ during the late Holocene. Holocene (ISSN: 09596836) 21, 211–224. http://dx.doi.org/10.1177/0959683610378877,

Bauer, A., 1968. Missions aeriennes de reconnaissance au Groenland 1957–1958; observations aeriennes et terrestres, exploitation des photographies aeriennes, determination des vitesses des glaciers velant dans Disko Bugt et Umanak Fjord. Meddelelser om Grønland 173 (3), 116.

Benn, D.I., Cowton, T., Todd, J., Luckman, A., 2017. Glacier calving in greenland. Curr. Clim. Change Rep. (ISSN: 21986061) 3, 282–290. http://dx.doi.org/10.1007/S40641-017-0070-1, URL https://link.springer.com/article/10.1007/s40641-017-0070-1.

Bondzio, J.H., Morlighem, M., Seroussi, H., Kleiner, T., Rückamp, M., Mouginot, J., Moon, T., Larour, E.Y., Humbert, A., 2017. The mechanisms behind Jakobshavn Isbrae's acceleration and mass loss: A 3-D thermomechanical model study. Geophys. Res. Lett. (ISSN: 00948276) 44, 6252–6260. http://dx.doi.org/10.1002/2017GL073309.

Bondzio, J.H., Morlighem, M., Seroussi, H., Wood, M.H., Mouginot, J., 2018. Control of ocean temperature on Jakobshavn Isbræ's present and future mass loss. Geophys. Res. Lett. (ISSN: 1944-8007) 45, 12,912–12,921. http://dx.doi.org/10.1029/2018GL079827, URL https://agupubs.onlinelibrary.wiley.com/doi/10.1029/2018GL079827.

Bondzio, J.H., Seroussi, H., Morlighem, M., Kleiner, T., Rückamp, M., Humbert, A., Larour, E.Y., 2016. Modelling calving front dynamics using a level-set method: application to Jakobshavn Isbræ, West Greenland. Cryosphere (ISSN: 1994-0424) 10, 497–510. http://dx.doi.org/10.5194/tc-10-497-2016.

Born, A., Robinson, A., 2021. Modeling the greenland englacial stratigraphy. Cryosphere 15, 4539–4556. http://dx.doi.org/10.5194/tc-15-4539-2021.

Briner, J., McKay, N., Axford, Y., Bennike, O., Bradley, R., de Vernal, A., Fisher, D., Francus, P., Fréchette, B., Gajewski, K., Jennings, A., Kaufman, D., Miller, G., Rouston, C., Wagner, B., 2016. Holocene climate change in Arctic Canada and Greenland. Quat. Sci. Rev. (ISSN: 0277-3791) 147, 340–364. http://dx.doi.org/10.1016/j.quascirev.2016.02.010.

Briner, J., Stewart, H., Young, N., Philipps, W., Losee, S., 2010. Using proglacial-threshold lakes to constrain fluctuations of the Jakobshavn Isbræ ice margin, western Greenland, during the Holocene. Quat. Sci. Rev. (ISSN: 0277-3791) 29, 3861–3874. http://dx.doi.org/10.1016/J.QUASCIREV.2010.09.005.

Briner, J., Young, N., Thomas, E., Stewart, H., Losee, S., Truex, S., 2011. Varve and radiocarbon dating support the rapid advance of Jakobshavn Isbræ during the Little Ice Age. Quat. Sci. Rev. (ISSN: 0277-3791) 30 (19), 2476–2486. http://dx.doi.org/10.1016/j.quascirev.2011.05.017, URL https://www.sciencedirect.com/science/article/pii/S0277379111001636.

Budd, W.F., Keage, P.L., Blundy, N.A., 1979. Empirical studies of ice sliding. J. Glaciol. (ISSN: 0022-1430) 23, 157–170. http://dx.doi.org/10.3189/S0022143000029804.

Catania, G.A., Stearns, L.A., Moon, T.A., Enderlin, E.M., Jackson, R.H., 2020. Future evolution of Greenland's marine-terminating outlet glaciers. J. Geophys. Res.: Earth Surf. (ISSN: 21699011) 125, http://dx.doi.org/10.1029/2018JF004873, URL https://agupubs.onlinelibrary.wiley.com/doi/10.1029/2018JF004873.

Choi, Y., Morlighem, M., Wood, M., Bondzio, J.H., 2018. Comparison of four calving laws to model Greenland outlet glaciers. Cryosphere (ISSN: 19940424) 12, 3735–3746. http://dx.doi.org/10.5194/TC-12-3735-2018.

Csatho, B., Schenk, T., Van Der Veen, C., Krabill, W.B., 2008. Intermittent thinning of Jakobshavn Isbræ, West Greenland, since the Little Ice Age. J. Glaciol. 54 (184), 131–144. http://dx.doi.org/10.3189/002214308784409035.

Cuffey, K.M., Paterson, W.S.B., 2010. The Physics of Glaciers, fourth ed. Elsevier Science & Technology Books, ISBN: 9780080919126, p. 704.

Fan, S., Hager, T.F., Prior, D.J., Cross, A.J., Goldsby, D.L., Qi, C., Negrini, M., Wheeler, J., 2020. Temperature and strain controls on ice deformation mechanisms: insights from the microstructures of samples deformed to progressively higher strains at −10, −20 and −30 °C. Cryosphere 14 (11), 3875–3905. http://dx.doi.org/10.5194/tc-14-3875-2020, URL https://tc.copernicus.org/articles/14/3875/2020/.

Fettweis, X., Box, J.E., Agosta, C., Amory, C., Kittel, C., Lang, C., As, D.V., Machguth, H., Gallée, H., 2017. Reconstructions of the 1900–2015 Greenland ice sheet surface mass balance using the regional climate MAR model. Cryosphere (ISSN: 19940424) 11, 1015–1033. http://dx.doi.org/10.5194/TC-11-1015-2017.

Gerber, T.A., Lilien, D.A., Rathmann, N.M., Franke, S., Young, T.J., Valero-Delgado, F., Ershadi, M.R., Drews, R., Zeising, O., Humbert, A., et al., 2023. Crystal orientation fabric anisotropy causes directional hardening of the Northeast Greenland Ice Stream. Nature Commun. 14 (1), 2653.

Gladish, C.V., Holland, D.M., Rosing-Asvid, A., Behrens, J.W., Boje, J., 2015. Oceanic boundary conditions for Jakobshavn Glacier. Part I: Variability and renewal of Ilulissat Icefjord waters, 2001-14. J. Phys. Oceanogr. (ISSN: 15200485) 45, 3–32. http://dx.doi.org/10.1175/JPO-D-14-0044.1.

Helsen, M.M., van de Wal, R.S.W., van den Broeke, M.R., van de Berg, W.J., Oerlemans, J., 2012. Coupling of climate models and ice sheet models by surface mass balance gradients: application to the Greenland Ice Sheet. Cryosphere (ISSN: 1994-0424) 6, 255–272. http://dx.doi.org/10.5194/tc-6-255-2012.

Joughin, I., Shean, D.E., Smith, B.E., Floricioiu, D., 2020. A decade of variability on Jakobshavn Isbræ: Ocean temperatures pace speed through influence on mélange rigidity. Cryosphere (ISSN: 19940424) 14, 211–227. http://dx.doi.org/10.5194/TC-14-211-2020.

Kajanto, K., Seroussi, H., de Fleurian, B., Nisancioglu, K.H., 2020. Present day Jakobshavn Isbræ close to the Holocene minimum extent. Quat. Sci. Rev. (ISSN: 02773791) 246, http://dx.doi.org/10.1016/j.quascirev.2020.106492.

Kajanto, K., Straneo, F., Nisancioglu, K., 2023. Impact of icebergs on the seasonal submarine melt of Sermeq Kujalleq. Cryosphere 17 (1), 371–390. http://dx.doi.org/10.5194/tc-17-371-2023, URL https://tc.copernicus.org/articles/17/371/2023/.

Khazendar, A., Fenty, I.G., Carroll, D., Gardner, A., Lee, C.M., Fukumori, I., Wang, O., Zhang, H., Seroussi, H., Moller, D., Noël, B.P.Y., van den Broeke, M.R., Dinardo, S., Willis, J., 2019. Interruption of two decades of Jakobshavn Isbrae acceleration and thinning as regional ocean cools. Nat. Geosci. (ISSN: 1752-0894) 12, 277–283. http://dx.doi.org/10.1038/s41561-019-0329-3.

Kjær, K.H., Bjørk, A.A., Kjeldsen, K.K., Hansen, E.S., Andresen, C.S., Siggaard-Andersen, M.L., Khan, S.A., Søsndergaard, A.S., Colgan, W., Schomacker, A., Woodroffe, S., Funder, S., Rouillard, A., Jensen, J.F., Larsen, N.K., 2022. Glacier response to the Little Ice Age during the Neoglacial cooling in Greenland. Earth-Sci. Rev. (ISSN: 0012-8252) 227, 103984. http://dx.doi.org/10.1016/J.EARSCIREV.2022.103984.

Kjeldsen, K.K., Korsgaard, N.J., Bjø rk, A.A., Khan, S.A., Box, J.E., Funder, S., Larsen, N.K., Bamber, J.L., Colgan, W., Van Den Broeke, M., et al., 2015. Spatial and temporal distribution of mass loss from the greenland ice sheet since AD 1900. Nature 528 (7582), 396–400.

Kobashi, T., Kawamura, K., Severinghaus, J.P., Barnola, J.-M., Nakaegawa, T., Vinther, B.M., Johnsen, S.J., Box, J.E., Kobashi, C.., Kawamura, K., Severinghaus, J.P., Barnola, J.-M., Nakaegawa, T., Vinther, B.M., Johnsen, S.J., Box, J.E., 2011. High variability of Greenland surface temperature over the past 4000 years estimated from trapped air in an ice core. Geophys. Res. Lett. (ISSN: 1944-8007) 38, http://dx.doi.org/10.1029/2011GL049444, URL https://agupubs.onlinelibrary.wiley.com/doi/10.1029/2011GL049444.

Larour, E., Seroussi, H., Morlighem, M., Rignot, E., 2012. Continental scale, high order, high spatial resolution, ice sheet modeling using the Ice Sheet System Model (ISSM). J. Geophys. Res.: Earth Surf. (ISSN: 01480227) 117, http://dx.doi.org/10.1029/2011JF002140.

Lecavalier, B.S., Milne, G.A., Simpson, M.J.R., Wake, L., Huybrechts, P., Tarasov, L., Kjeldsen, K.K., Funder, S., Long, A.J., Woodroffe, S., Dyke, A.S., Larsen, N.K., 2014. A model of Greenland ice sheet deglaciation constrained by observations of relative sea level and ice extent. Quat. Sci. Rev. (ISSN: 0277-3791) 102, 54–84. http://dx.doi.org/10.1016/J.QUASCIREV.2014.07.018.

Long, A., Roberts, D., Dawson, S., 2006. Early Holocene history of the west Greenland Ice Sheet and the GH-8.2 event. Quat. Sci. Rev. (ISSN: 0277-3791) 25, 904–922. http://dx.doi.org/10.1016/J.QUASCIREV.2005.07.002.

MacAyeal, D.R., 1989. Large-scale ice flow over a viscous basal sediment: Theory and application to ice stream B, Antarctica. J. Geophys. Res.: Solid Earth (ISSN: 01480227) 94, 4071–4087. http://dx.doi.org/10.1029/JB094iB04p04071.

MacGregor, J.A., Colgan, W.T., Fahnestock, M.A., Morlighem, M., Catania, G.A., Paden, J.D., Gogineni, S.P., 2016. Ice sheets: Holocene deceleration of the Greenland Ice Sheet. Science (ISSN: 10959203) 351, 590–593. http://dx.doi.org/10.1126/SCIENCE.AAB1702/SUPPL_FILE/MACGREGOR.SM.PDF, URL https://www.science.org/doi/10.1126/science.aab1702.

Martos, Y.M., Jordan, T.A., Catalán, M., Jordan, T.M., Bamber, J.L., Vaughan, D.G., 2018. Geothermal heat flux reveals the iceland hotspot track underneath Greenland. Geophys. Res. Lett. (ISSN: 1944-8007) 45, 8214–8222. http://dx.doi.org/10.1029/2018GL078289, URL https://agupubs.onlinelibrary.wiley.com/doi/10.1029/2018GL078289.

Morland, L., 1987. Unconfined ice-shelf flow. Dyn. West Antarct. Ice Sheet 99–116. http://dx.doi.org/10.1007/978-94-009-3745-1_6.

Morlighem, M., Bondzio, J., Seroussi, H., Rignot, E., Larour, E., Humbert, A., Rebuffi, S., 2016. Modeling of Store Gletscher's calving dynamics, West Greenland, in response to ocean thermal forcing. Geophys. Res. Lett. (ISSN: 0094-8276) 43, 2659–2666. http://dx.doi.org/10.1002/2016GL067695.

Morlighem, M., Williams, C.N., Rignot, E., An, L., Arndt, J.E., Bamber, J.L., Catania, G., Chauché, N., Dowdeswell, J.A., Dorschel, B., Fenty, I., Hogan, K., Howat, I., Hubbard, A., Jakobsson, M., Jordan, T.M., Kjeldsen, K.K., Millan, R., Mayer, L., Mouginot, J., Noël, B.P.Y., O'Cofaigh, C., Palmer, S., Rysgaard, S., Seroussi, H., Siegert, M.J., Slabon, P., Straneo, F., van den Broeke, M.R., Weinrebe, W., Wood, M., Zinglersen, K.B., 2017. BedMachine v3: Complete bed topography and ocean bathymetry mapping of Greenland from multibeam echo sounding combined with mass conservation. Geophys. Res. Lett. (ISSN: 00948276) 44, 11,051–11,061. http://dx.doi.org/10.1002/2017GL074954.

Morlighem, M., Wood, M., Seroussi, H., Choi, Y., Rignot, E., 2019. Modeling the response of northwest Greenland to enhanced ocean thermal forcing and subglacial discharge. Cryosphere (ISSN: 19940424) 13, 723–734. http://dx.doi.org/10.5194/TC-13-723-2019.

Moros, M., Lloyd, J.M., Perner, K., Krawczyk, D., Blanz, T., de Vernal, A., Ouellet-Bernier, M.-M., Kuijpers, A., Jennings, A.E., Witkowski, A., Schneider, R., Jansen, E., 2016. Surface and sub-surface multi-proxy reconstruction of middle to late Holocene palaeoceanographic changes in Disko Bugt, West Greenland. Quat. Sci. Rev. (ISSN: 0277-3791) 132, 146–160. http://dx.doi.org/10.1016/J.QUASCIREV.2015.11.017.

Mouginot, J., Rignot, E., Bjørk, A.A., van den Broeke, M., Millan, R., Morlighem, M., Noël, B., Scheuchl, B., Wood, M., 2019. Forty-six years of Greenland Ice Sheet mass balance from 1972 to 2018. Proc. Natl. Acad. Sci. USA (ISSN: 10916490) 116, 9239–9244. http://dx.doi.org/10.1073/PNAS.1904242116.

Murray, T., Scharrer, K., Selmes, N., Booth, A.D., James, T.D., Bevan, S.L., Bradley, J., Cook, S., Llana, L.C., Drocourt, Y., Dyke, L., Goldsack, A., Hughes, A.L., Luckman, A.J., McGovern, J., 2015. Extensive Retreat of Greenland Tidewater Glaciers, 2000–2010. Arct. Antarct. Alp. Res. (ISSN: 19384246) 47, 427–447. http://dx.doi.org/10.1657/AAAR0014-049, URL https://www.tandfonline.com/doi/abs/10.1657/AAAR0014-049.

Nowicki, S., Goelzer, H., Seroussi, H., Payne, A.J., Lipscomb, W.H., Abe-Ouchi, A., Agosta, C., Alexander, P., Asay-Davis, X.S., Barthel, A., Bracegirdle, T.J., Cullather, R., Felikson, D., Fettweis, X., Gregory, J.M., Hattermann, T., Jourdain, N.C., Kuipers Munneke, P., Larour, E., Little, C.M., Morlighem, M., Nias, I., Shepherd, A., Simon, E., Slater, D., Smith, R.S., Straneo, F., Trusel, L.D., van den Broeke, M.R., van de Wal, R., 2020. Experimental protocol for sea level projections from ISMIP6 stand-alone ice sheet models. Cryosphere 14 (7), 2331–2368. http://dx.doi.org/10.5194/tc-14-2331-2020, URL https://tc.copernicus.org/articles/14/2331/2020/.

Plach, A., Nisancioglu, K.H., clec'h, S.L., Born, A., Langebroek, P.M., Guo, C., Imhof, M., Stocker, T.F., 2018. Eemian Greenland SMB strongly sensitive to model choice. Clim. Past (ISSN: 1814-9332) 14, 1463–1485. http://dx.doi.org/10.5194/cp-14-1463-2018.

Rieckh, T., Born, A., Robinson, A., Gülle, G., 2023. Introducing ELSA v2.0: An isochronal model for ice-sheet layer tracing. Geosci. Model Dev. (in preparation).

Robinson, A., Alvarez-Solas, J., Montoya, M., Goelzer, H., Greve, R., Ritz, C., 2020. Description and validation of the ice-sheet model Yelmo (version 1.0). Geosci. Model Dev. (ISSN: 19919603) 13, 2805–2823. http://dx.doi.org/10.5194/GMD-13-2805-2020.

Seroussi, H., Morlighem, M., Larour, E., Rignot, E., Khazendar, A., 2014. Hydrostatic grounding line parameterization in ice sheet models. Cryosphere (ISSN: 1994-0424) 8, 2075–2087. http://dx.doi.org/10.5194/tc-8-2075-2014.

Seroussi, H., Morlighem, M., Rignot, E., Khazendar, A., Larour, E., Mouginot, J., 2013. Dependence of century-scale projections of the Greenland ice sheet on its thermal regime. J. Glaciol. (ISSN: 0022-1430) 59, 1024–1034. http://dx.doi.org/10.3189/2013JoG13J054.

Seroussi, H., Nakayama, Y., Larour, E., Menemenlis, D., Morlighem, M., Rignot, E., Khazendar, A., 2017. Continued retreat of Thwaites Glacier, West Antarctica, controlled by bed topography and ocean circulation. Geophys. Res. Lett. (ISSN: 19448007) 44, 6191–6199. http://dx.doi.org/10.1002/2017GL072910, URL https://agupubs.onlinelibrary.wiley.com/doi/10.1002/2017GL072910.

Shapiro, N.M., Ritzwoller, M.H., 2004. Inferring surface heat flux distributions guided by a global seismic model: particular application to Antarctica. Earth Planet. Sci. Lett. (ISSN: 0012-821X) 223, 213–224. http://dx.doi.org/10.1016/J.EPSL.2004.04.011.

Stoll, N., Eichler, J., Hörhold, M., Shigeyama, W., Weikusat, I., 2021. A review of the microstructural location of impurities in polar ice and their impacts on deformation. Front. Earth Sci. 8, 615613.

Vinther, B.M., Buchardt, S.L., Clausen, H.B., Dahl-Jensen, D., Johnsen, S.J., Fisher, D.A., Koerner, R.M., Raynaud, D., Lipenkov, V., Andersen, K.K., Blunier, T., Rasmussen, S.O., Steffensen, J.P., Svensson, A.M., 2009. Holocene thinning of the Greenland ice sheet. Nature (ISSN: 0028-0836) 461, 385–388. http://dx.doi.org/10.1038/nature08355.

Wangner, D.J., Jennings, A.E., Vermassen, F., Dyke, L.M., Hogan, K.A., Schmidt, S., Kjær, K.H., Knudsen, M.F., Andresen, C.S., 2018. A 2000-year record of ocean influence on Jakobshavn Isbræ calving activity, based on marine sediment cores. Holocene (ISSN: 0959-6836) 28, 1731–1744. http://dx.doi.org/10.1177/0959683618788701, URL http://journals.sagepub.com/doi/10.1177/0959683618788701.

Weidick, A., Bennike, O., 2007. Quaternary Glaciation History and Glaciology of Jakobshavn Isbrae and the Disko Bugt Region, West Greenland : A Review. Geological Survey of Denmark and Greenland, ISBN: 9788778712073, p. 78.

Weidick, A., Mikkelsen, N., Mayer, C., Podlech, S., 2004. Jakobshavn Isbræ, West Greenland: the 2002–2003 collapse and nomination for the UNESCO World Heritage List. GEUS Bull. 4, 85–88.

Weidick, A., Oerter, H., Reeh, N., Thomsen, H.H., Thorning, L., 1990. The recession of the Inland Ice margin during the Holocene climatic optimum in the Jakobshavn Isfjord area of West Greenland. Palaeogeogr. Palaeoclimatol. Palaeoecol. (ISSN: 0031-0182) 82 (3), 389–399. http://dx.doi.org/10.1016/S0031-0182(12)80010-1, URL https://www.sciencedirect.com/science/article/pii/S0031018212800101.

Wood, M., Rignot, E., Fenty, I., An, L., Bjørk, A., van den Broeke, M., Cai, C., Kane, E., Menemenlis, D., Millan, R., Morlighem, M., Mouginot, J., Noël, B., Scheuchl, B., Velicogna, I., Willis, J.K., Zhang, H., 2021. Ocean forcing drives glacier retreat in Greenland. Sci. Adv. (ISSN: 23752548) 7, http://dx.doi.org/10.1126/SCIADV.ABA7282, URL https://www.science.org/doi/full/10.1126/sciadv.aba7282.